Theory-Guided Design and Machine-Learning Identification of a Nested Nodal-Surface Semimetal in the Carbon Allotrope bct-C12

Shuaihua Zhang, Silei Guo, Jingxiang Liu, Baoxin Hu, Yanling Wu,* and Jun Li†
State Key Laboratory of Metastable Materials Science and Technology, Hebei Key Laboratory of Microstructural Material Physics, School of Science, Yanshan University, Qinhuangdao, 066004, China.

Extending the Dirac physics of two-dimensional graphene into three-dimensional (3D) carbon allotropes with higher-dimensional band degeneracies remains a central challenge in topological materials science. Here, we propose a general symmetry-engineering principle that systematically transforms graphene's Dirac cone into a 3D nodal surface via controlled layering and registry shift, and employ this principle to guide a machine-learning-accelerated inverse design. By integrating a crystal diffusion variational autoencoder (CDVAE) with CrystalFormer, we identify a body-centered tetragonal carbon structure (previously reported as bct-C12) which we also name Netsene. First-principles calculations reveal that this known material hosts a previously unrecognized nested nodal-surface system near the Fermi level, protected by non-symmorphic symmetries, alongside Dirac-like linear crossings with Fermi velocities comparable to graphene. Its non-trivial bulk topology, verified by Wilson-loop and Berry-phase calculations, is expected to manifest in drumhead surface states, including a nearly flat band. Netsene thus provides a structurally robust, bulk platform that combines high Fermi velocities comparable to graphene, topological nodal surfaces, and a high density of states that may foster correlation effects worthy of future study, demonstrating the power of theory-guided, machine-learning-accelerated identification for engineering exotic topological quantum phases.

Keywords: Carbon allotrope; Topological band theory; Machine-learning inverse design; Graphene layering

PACS numbers: 71.20.-b, 73.20.-r, 81.05.Uw

I. INTRODUCTION

The experimental realization of graphene has established two-dimensional (2D) Dirac semimetals as a cornerstone of modern condensed matter physics, unveiling massless relativistic quasiparticles and exceptional carrier mobilities [1, 2]. A central pursuit in topological materials science is to extend such Dirac physics into three-dimensions (3D), where higher-dimensional band degeneracies can emerge, such as one-dimensional (1D) nodal lines and 2D nodal surfaces [3, 4]. Among these, nodal surfaces, across which two bands remain degenerate on an entire 2D manifold in momentum space, are particularly intriguing. They can host extended regions of high density of states (DOS), potentially fostering enhanced electronic correlations and exotic transport phenomena [5]. However, realizing clean, robust nodal surfaces near the Fermi level (E_F) in stable materials remains a significant challenge. Their existence often demands specific, non-symmorphic crystal symmetries and a delicate balance of electronic interactions, making both their rational design and experimental realization difficult [6].

Elemental carbon, with its weak spin-orbit coupling (SOC) and extraordinary structural diversity (sp, sp^2, sp^3 hybridization), offers an ideal materials platform for engineering topological band structures [7, 8]. The weak SOC preserves band degeneracies protected by spacetime inversion symmetry, while carbon's versatile bonding enables the construction of complex 3D networks with tailored symmetries. This raises a fundamental question: *Can graphene's Dirac cones be rationally transformed into symmetry-protected nodal surfaces in a 3D carbon allotrope?*

In this work, we answer this question affirmatively by proposing and validating a general symmetry-engineering principle that systematically elevates the dimensionality of band degeneracies. Our strategy unfolds in three conceptual steps: (i) reducing the in-plane hexagonal symmetry of graphene to break the equivalence of hopping directions, promoting the zero-dimensional (0D) Dirac point into a 1D nodal line; (ii) introducing a controlled half-lattice-constant registry shift between graphene layers to extend this nodal line; and (iii) permanently "fixing" the shifted layers with a covalent sp^3 carbon network, which simultaneously stabilizes a body-centered tetragonal structure and activates non-symmorphic symmetries that enforce a 2D nodal surface. Rather than relying on trial-and-error, we translate this design principle into a target for machine-learning-accelerated inverse design. By combining a crystal diffusion variational autoencoder (CDVAE) [9] with CrystalFormer [10], we efficiently navigate the vast chemical space of carbon allotropes and identify a low-energy phase that perfectly embodies our design.

The crystal structure that satisfies the above design criteria was independently identified by our machine-

* ylwu@ysu.edu.cn
† ljcj007@ysu.edu.cn

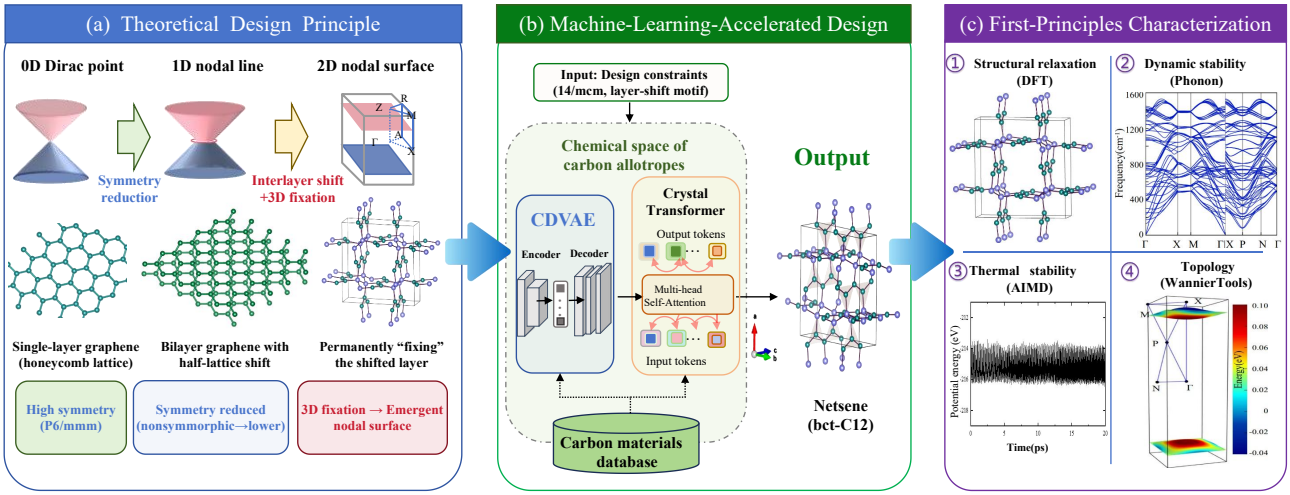


FIG. 1: Schematic overview of the integrated research methodology. (a) Three-step symmetry-engineering design principle for transforming a 2D Dirac cone into a 3D nodal surface. (b) Workflow of the machine-learning-accelerated inverse design combining a CDVAE and CrystalFormer. (c) Key first-principles characterization methods used to validate the predicted structure and its topological properties.

learning pipeline as the lowest-energy candidate. During the course of this work, we became aware that this structure had been previously reported as bct-C12 [11]. Those earlier works focused on its anisotropic Dirac fermions and mechanical properties, but the possibility of a nested nodal surface remained unexplored. Here, we re-examine this material, through our symmetry-engineering lens and first-principles calculations, revealing a rich nested nodal-surface system that was not previously recognized. We name this material "Netsene", combining "net" (reflecting its three-dimensional network-like framework) with the suffix "-sene", a convention used for carbon allotropes with extended π-conjugation (such as graphene and graphyne). Netsene crystallizes in the $I4/mcm$ space group and exhibits remarkable properties: exceptionally high stiffness along the c-axis ($C_{33} = 1134.2$ GPa), Dirac-like linear crossings with Fermi velocities comparable to graphene ($\sim 9 \times 10^5$ m/s), and a complex nodal surface giving rise to drumhead surface states including a nearly flat band. This material thus shares conceptual similarities with magic-angle twist bilayer graphene (TBG) [12–14] in that both exhibit flat-band features near the Fermi level, although the origin of the flat bands is fundamentally different (translational shift versus rotational misorientation). It thus provides a structurally robust bulk platform in which correlation effects may be investigated in future work.

II. METHODS

A. Theoretical Design Principle

Our strategy to engineer a 3D nodal-surface semimetal from graphene is a three step symmetry engineering procedure that systematically raises the dimensionality of the band degeneracy. We outline each step below with analytical model derivations.

Step 1: From 0D Dirac point to 1D nodal line via in-plane symmetry reduction. Monolayer graphene has a honeycomb lattice with two atoms per unit cell. In the nearest-neighbor tight-binding approximation, its Hamiltonian in momentum space is

$$H_0(\mathbf{k}) = \begin{pmatrix} 0 & tf(\mathbf{k}) \\ tf^*(\mathbf{k}) & 0 \end{pmatrix}, \quad f(\mathbf{k}) = \sum_{j=1}^{3} e^{i\mathbf{k}\cdot\delta_j}, \qquad (1)$$

where t is the hopping integral and δ_j are the three nearest-neighbor vectors. Expanding around the K point $\mathbf{K} = (4\pi/3a, 0)$ yields the massless Dirac Hamiltonian

$$H_{\text{Dirac}} = v_F(k_x\sigma_x + k_y\sigma_y), \qquad (2)$$

with Fermi velocity $v_F = \sqrt{3}ta/2$. This is a 0D point degeneracy. If we preserve the honeycomb connectivity but lower the in-plane symmetry from hexagonal to orthorhombic (space group $p2/m$), the equivalence between the three hopping directions is lifted. The effective Hamiltonian near the former K point becomes

$$H_{\text{ortho}}(\mathbf{q}) = v_x q_x \sigma_x + v_y q_y \sigma_y, \qquad (3)$$

where $v_x \neq v_y$ in general. In an isolated 2D system this remains a point node, but when interlayer coupling is introduced in the next step, the reduced symmetry can promote it into a line degeneracy.

Step 2: From 1D nodal line to 2D nodal surface via interlayer registry shift. Consider two such graphene layers stacked with a relative shift $\mathbf{d} = (a/2, 0)$ along the armchair direction. The interlayer coupling is modeled by a hopping matrix between the layers. In the basis of the

two layers (each with A/B sublattices), the total bilayer Hamiltonian is

$$H_{\text{bilayer}}(\mathbf{k}) = \begin{pmatrix} H_0(\mathbf{k}) & T(\mathbf{k}) \\ T^\dagger(\mathbf{k}) & H_0(\mathbf{k}) \end{pmatrix}, \tag{4}$$

where $T(\mathbf{k})$ is the interlayer hopping matrix. For the armchair shift $(a/2, 0)$, the diagonal interlayer hopping becomes momentum dependent and can vanish along certain lines in the Brillouin zone, generating a protected nodal line. The low-energy effective model around such a nodal line is

$$H_{\text{line}}(\mathbf{q}) = v_\perp(q_1\sigma_x + q_2\sigma_y) + w(q_1, q_2)\sigma_0, \tag{5}$$

where q_1, q_2 are momenta perpendicular to the line, and w tilts the cone. The line itself is protected by a $\mathbb{Z}_2$ invariant (Berry phase π) when time-reversal and sublattice symmetries are present.Such nodal lines have been theoretically predicted in several three-dimensional carbon allotropes [15–19].

Step 3: Permanent 3D fixation and symmetry-protected nodal surface. To extend the nodal line into a 2D nodal surface, we permanently connect the two shifted layers with an additional carbon network that forms a square lattice. This covalently "fixes" the shifted geometry into a bulk structure. The resulting crystal is body-centered tetragonal (bct) with space group *I4/mcm* (No. 140). This space group possesses nonsymmorphic symmetry operations, notably a screw axis $\{C_{2z}|(\frac{1}{2}, \frac{1}{2}, 0)\}$ and a glide mirror $\{M_y|(\frac{1}{2}, \frac{1}{2}, 0)\}$, which are essential for stabilizing the nodal surface. In the 3D periodic structure, the interlayer coupling becomes k_z-dependent. The effective Hamiltonian near the former nodal line can be written as

$$H_{\text{3D}}(\mathbf{k}) = \begin{pmatrix} \varepsilon_0(\mathbf{k}) & \Delta(\mathbf{k}) \\ \Delta^*(\mathbf{k}) & \varepsilon_0(\mathbf{k}) \end{pmatrix}, \tag{6}$$

where $\Delta(\mathbf{k})$ is the effective hybridization between the two shifted graphene subunits. Owing to the bct symmetry constraints, $\Delta(\mathbf{k})$ is forced to vanish on a 2D manifold in the Brillouin zone,

$$\Delta(\mathbf{k}) = 0 \quad \Rightarrow \quad \text{nodal surface } \mathcal{S}. \tag{7}$$

This surface is not accidental but symmetry-enforced, and the degeneracy is topologically protected by a $\mathbb{Z}_2$ invariant derived from the Berry phase of loops encircling the surface [20]. The idea of chemically fixing shifted graphene layers into a stable 3D network is reminiscent of hydrogenated graphene (graphane), where sp^2 to sp^3 rehybridization leads to new electronic phases [21]. Recent experimental progress in fabricating graphene-on-diamond heterostructures [22] further supports the synthetic plausibility of such a phase. Thus, the search for a 3D nodal-surface semimetal reduces to identifying a stable carbon allotrope that realizes the symmetry conditions of the *I4/mcm* bct structure.

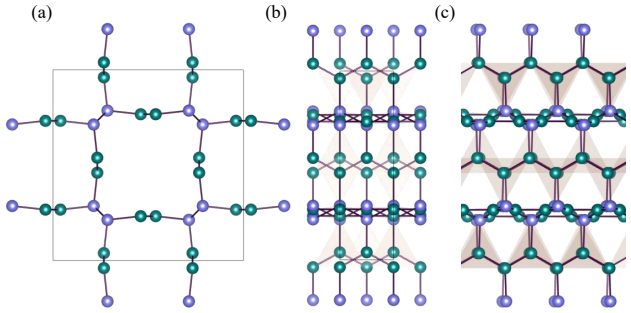


FIG. 2: (a) The conventional unit cell of **Netsene** viewed along the c-axis, showing the layered arrangement. C1 (sp^2-like) and C2 (sp^3-like) atoms are shown in green and blue, respectively. (b) Side view along the a-axis, highlighting the stacking sequence of four distinct layers. (c) Projection along the a-axis, clearly showing the armchair-direction shift between adjacent layers. The (110) plane forms the distorted honeycomb lattice.

B. Machine-Learning-Accelerated Inverse Design

The design principle derived in Section II A establishes a clear structural target: a body-centered tetragonal network with half-shifted graphene-like layers. To efficiently navigate the vast space of carbon allotropes compatible with this target, we employed a deep generative framework that integrates CDVAE [9] with CrystalFormer architecture [10].

The CDVAE generates candidate structures by learning the distribution of known carbon allotropes and performing diffusion-based sampling in the latent space. The generated candidates are then passed to the CrystalFormer, which serves a dual purpose: (i) it enforces the required *I4/mcm* space-group symmetry and the structural motif (layered network with armchair registry shift), and (ii) it estimates the formation energy of each candidate. This two-stage pipeline allows us to filter out high-energy or symmetry-incompatible structures and rank the remaining candidates by their energetic stability.

Starting from a training set comprising about two thousand 3D carbon networks drawn from the Materials Project [23], the SACADA database [24], and recent theoretical literature, the generative process produced a pool of structures satisfying the prescribed space group and bonding topology. After discarding duplicates and structures with unrealistic bond lengths, seven candidates compatible with the body-centered tetragonal lattice were retained. Among these seven, we selected the one that best fulfilled our design criteria: a layered network with a half-lattice-constant armchair shift between adjacent graphene-like sheets.

It was brought to our attention at the preprint stage that the same atomic arrangement had been independently reported as bct-C12 by Dong *et al.* [11],

who focused on its stability, mechanical properties, and anisotropic Dirac fermions. We emphasize that our screening procedure was performed without seeding known candidate structures and was guided exclusively by the symmetry-engineering principle and the energetic ranking from the generative model. The resulting lowest-energy structure was later identified as bct-C12 through independent literature mining, confirming that our physics-driven generative model successfully converged to a chemically and topologically optimal configuration.

C. First-Principles Calculations

All first-principles calculations in this work were performed using the Quantum ESPRESSO (QE) [25]. The electronic exchange-correlation interactions were treated within the generalized gradient approximation (GGA) as parameterized by the Perdew-Burke-Ernzerhof (PBE) functional [26]. Optimized norm-conserving Vanderbilt pseudopotentials were employed with a kinetic energy cutoff of 80 Ry for the wavefunctions and 600 Ry for the charge density, ensuring excellent convergence for the mixed sp^2–sp^3 carbon networks. For the pristine bulk unit cell of Netsene, Monkhorst-Pack $6 \times 6 \times 20$ k-point mesh was used for Brillouin zone sampling. Structural relaxations were carried out by fully optimizing both atomic coordinates and lattice vectors until the total energy change between successive steps was below 10^{-8} Ry, and forces on each atom were less than 10^{-6} Ry/Bohr.

Phonon dispersions were calculated using density functional perturbation theory (DFPT) as implemented in QE to assess dynamic stability. *Ab initio* molecular dynamics (AIMD) simulations were performed at 500 K for 20 ps to verify thermal stability. Maximally localized Wannier functions (MLWFs) for the carbon p orbitals were constructed using the Wannier90 code [27], yielding a faithful tight-binding Hamiltonian for the surface state calculations. Topological invariants were evaluated through Wilson-loop calculations of the Wannier charge centers (WCCs), irreducible representation analysis of the band crossings, and Berry phase calculations on closed loops encircling the nodal surface features [20, 28–30].

III. RESULTS AND DISCUSSION

A. Crystal Structure and Stability of Netsene

The crystal structure we identified, Netsene, Its optimized equilibrium lattice parameters are $a = b = 8.6913$ Å and $c = 2.4674$ Å. The conventional unit cell contains 24 carbon atoms occupying two inequivalent Wyckoff positions: C1 at $8k$ $(0.03926, 0.73720, 0.5)$ and C2 at $4h$ $(0.71365, 0.78635, 0.5)$. The crystal structure is illustrated in Fig. 2.

The structure faithfully embodies the three-step design principle presented in Section II A. In the top view along the c-axis [Fig. 2(a)], the carbon network displays a characteristic "well"-shaped pattern. The two parallel arms of this "well", one horizontal pair or, equivalently, one vertical pair, constitute the two half-shifted graphene-like layers derived from Step 2. These layers are held in registry by C2 atoms (blue spheres, $4h$ site) that adopt sp^3-like hybridization and form linear pillars along the c-direction. These sp^3 connectors correspond exactly to the "additional carbon network that forms a square lattice" invoked in Step 3 of the design principle, thereby permanently fixing the shifted geometry into a three-dimensional covalent framework. The sp^2-like C1 atoms (green spheres, $8k$ site) constitute the distorted honeycomb rings within each layer.

As shown in Figs. 2(a) and 2(b), the structure faithfully realizes our design: it consists of graphene-like layers stacked along the c-axis with a specific half-lattice-constant shift along the armchair direction, clearly visualized in the a-axis projection of Fig. 2(c). This stacking pattern generates a 3D covalent network in which C1 atoms primarily exhibit sp^2-like hybridization, forming distorted hexagonal rings within the layers, while C2 atoms adopt an sp^3-like hybridization, serving as interlayer connectors. This mixed hybridization is key to the structure's 3D rigidity while preserving the π-electron network essential for the topological electronic structure.

The distorted honeycomb lattice in the (110) plane features three distinct bond lengths: C1–C1 = 1.410 Å, C1–C2 = 1.525 Å, and C2–C2 = 1.523 Å. Notably, the C1–C1 bond is slightly shorter than the C–C bond in graphene (1.42 Å), indicating in-plane bond strengthening, while the interlayer bonds (C1–C2, C2–C2) are considerably shorter than the sp^3 bond in diamond (1.55 Å), reflecting a highly cohesive 3D network.

We rigorously assessed the stability of Netsene through multiple complementary approaches. The calculated energy-volume curve per atom is shown in Fig. 3(a), alongside those of diamond, graphite, and several previously reported carbon allotropes. The cohesive energy per atom of Netsene is −8.969 eV, which lies between that of graphite (−9.045 eV) and diamond (−9.018 eV). This energetic positioning indicates that Netsene is a metastable phase: it is higher in energy than diamond and graphite, but notably more stable than other theoretically predicted phases, such as tr98, bct-C40, oC24, C60, bco-C16, and oC8 [7, 8, 31–34], as well as other metastable carbon allotropes like Graphynes [35] and Biphenylene networks [36]. Consequently, Netsene ranks among the most favorable low-energy metastable carbon allotropes predicted to date. This favorable energetic position suggests promising synthetic accessibility.

Phonon dispersion calculations, performed across the entire Brillouin zone using DFPT, are presented in Fig. 3(b). The absence of any imaginary frequency modes confirms the dynamic stability of Netsene, indicating that the structure resides at a genuine local minimum on

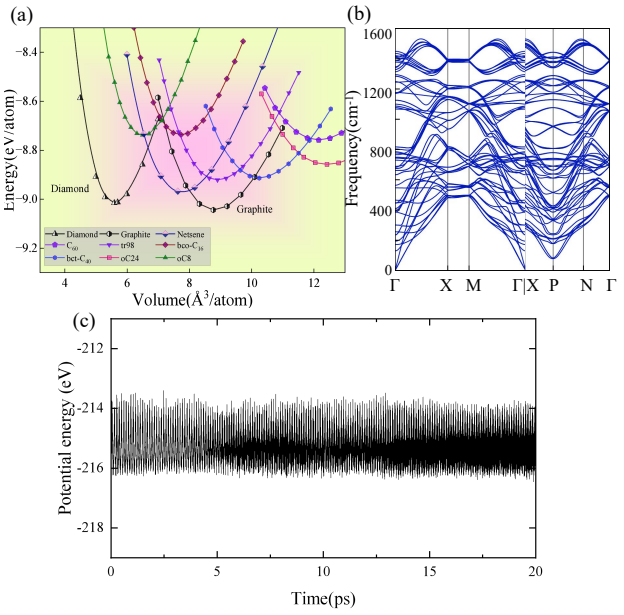


FIG. 3: (a) The energy–volume curve of Netsene, compared with diamond, graphite, and the previously reported oC8, bco-C16, oC24, bct-C40, C60, and tr98 structures. (b) Phonon band structures under zero pressure. The highest phonon frequency is approximately 1532 cm^{-1}, which is close to that of graphite (1610 cm^{-1})[37]. (c) Potential energy fluctuations during AIMD simulations at 500 K for 20 ps, confirming thermal stability.

the potential energy surface. The highest phonon frequency reaches approximately 1532 cm^{-1}, which is close to that of graphite (1610 cm^{-1}) and indicative of strong covalent bonding. Furthermore, AIMD simulations at 500 K [Fig. 3(c)] demonstrate excellent thermal stability: the structure remains intact with negligible fluctuations in total potential energy and no bond-breaking events throughout the 20 ps simulation, confirming that Netsene can maintain its structural integrity well above room temperature.

B. Mechanical Properties

The mechanical robustness of Netsene was quantified by calculating its full elastic constant tensor C_{ij}. For a tetragonal crystal (point group $4/mmm$), there are six independent elastic constants: C_{11}, C_{12}, C_{13}, C_{33}, C_{44}, and C_{66}. Our calculated values are listed in Table I, alongside those of diamond and graphite for comparison. All C_{ij} values satisfy the generalized Born-Huang stability criteria for a tetragonal system:

$$C_{11} > |C_{12}|,\ C_{44} > 0,\ C_{66} > 0,\ 2C_{13}^2 < C_{33}(C_{11} + C_{12}), \tag{8}$$

further corroborating its mechanical stability.

The derived bulk modulus B of Netsene is 290 GPa, comparable to that of graphite (280 GPa) but lower than diamond's 451 GPa, indicating substantial incompressibility for a low-density carbon framework. The shear modulus G (217 GPa) and Young's modulus E (522 GPa) are remarkably high, surpassing those of most known 3D carbon allotropes and many advanced ceramics. This places Netsene in the category of ultra-strong, lightweight materials.

Most strikingly, the value of $C_{33} = 1134.2$ GPa is exceptionally high, exceeding even the in-plane elastic constant of graphene ($C_{11} \sim 1100$ GPa). This reveals that Netsene possesses outstanding stiffness specifically along the crystallographic c-axis—the stacking direction. This unique anisotropy arises directly from the structural motif: the sp^3-bonded C2 connectors form nearly linear, highly rigid chains parallel to the c-axis, effectively bridging the sp^2 honeycomb layers. Netsene thus combines the in-plane strength characteristic of graphene with an unprecedented out-of-plane rigidity, a combination that is highly desirable for structural applications and that directly reflects the success of our "fixing" design strategy.

C. Electronic Structure and the Nested Nodal-Surface System

We now turn to the defining electronic feature of Netsene: its topological nodal-surface semimetal character. The electronic band structure along high-symmetry paths, calculated without SOC, is presented in Fig. 4(a). Netsene exhibits a clear semimetallic character, with multiple bands crossing the E_F. Two prominent linear band crossings are observed near E_F: one along the Γ–X path (denoted D_1), located at $k \approx 1.7953\,Å^{-1}$ and approximately 80 meV below E_F, and another near the M–Γ region (denoted D_2), located at $k \approx 4.2928\,Å^{-1}$.

A detailed linear fit to these crossings confirms their massless Dirac-fermion nature. The Fermi velocities extracted for D_1 are $v_F^{\rm val} \approx 9.03\times10^5$ m/s and $v_F^{\rm con} \approx 8.37\times10^5$ m/s, while those for D_2 are $v_F^{\rm val} \approx 9.05\times10^5$ m/s and $v_F^{\rm con} \approx 9.99\times10^5$ m/s. These values are on the same order of magnitude as the Fermi velocity of pristine graphene ($\sim 8.5\times10^5$ m/s) [40], suggesting that Netsene may exhibit carrier mobility comparable to graphene, a hallmark of high-performance electronic materials, although quantitative mobility predictions would require detailed scattering rate calculations beyond the current scope.

The overall DOS at E_F is finite but relatively low, characteristic of a semimetal [Fig. 4(b)]. The projected DOS reveals that the states near E_F are predominantly contributed by the p orbitals of both C1 and C2 atoms, confirming that the low-energy physics is governed by the π-bonding network inherited from the graphene-like layers.

Beyond these isolated Dirac-like points, the most striking feature of Netsene's electronic structure is the presence of a complex, extended degeneracy forming a nested

TABLE I: Calculated elastic constants C_{ij} (in GPa), bulk modulus B, shear modulus G, Young's modulus E (in GPa), and Poisson's ratio ν for Netsene, compared with diamond and graphite. All values are from PBE-DFT calculations for consistency.

Material	C_{11}	C_{33}	C_{44}	C_{66}	C_{12}	C_{13}	B	G	E	ν
Netsene	551.1	1134.2	278.7	70.1	98.2	165.4	290	217	522	0.2
Diamond [38]	1079	1079	578	578	124	124	451	535	1143	0.17
Graphite [39]	1109	38.7	4.95	4.5	139	0	280	4.2	12	0.49

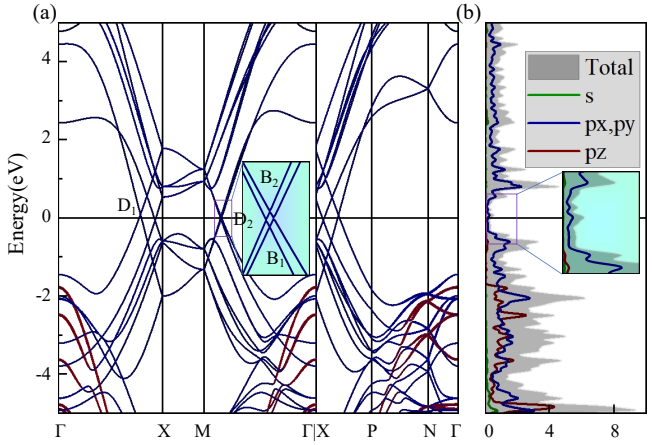


FIG. 4: (a) Electronic band structure of Netsene along high-symmetry lines. The inset zooms in on the linear crossings near D_2. (b) Total and atom-projected DOS. The E_F is set to zero.

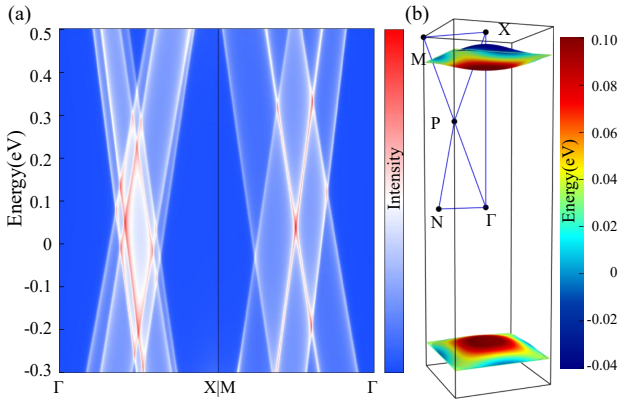


FIG. 5: (a) 3D visualization of the nested nodal-surface system around the E_F, showing the "double-bowl" shaped degeneracy manifolds. (b) Schematic of the constant-k_z evolution of the band crossings, illustrating how the nodal surfaces form and annihilate as a function of k_z.

nodal-surface system. This is visualized in the 3D band structure plot of Fig. 5(a), where a series of nearly flat bands intersect and overlap near E_F, creating 2D manifolds of band degeneracy in specific regions of the Brillouin zone.

Specifically, we identify four distinct nodal surfaces centered around $k_z \approx \pm 0.42\,(2\pi/c)$. The genesis and evolution of these degeneracies are elucidated by examining constant-k_z slices of the band structure. At $k_z = 0.39\,(2\pi/c)$, near the Γ point ($k_x = k_y = 0$), two pairs of bands approach each other, forming two separate linear crossings. As k_z increases to $0.42\,(2\pi/c)$, these four bands converge to a four-fold degenerate point precisely at Γ. Simultaneously, a separate four-fold degeneracy emerges at the zone boundary ($k_x = k_y = 0.5$). Upon further increasing k_z to $0.46\,(2\pi/c)$, the degeneracies split again into two Dirac-like points. This evolution, illustrated schematically in Fig. 5(b), creates a distinctive nested, "double-bowl" shaped nodal surface in the 3D Brillouin zone.

The origin of this robust nodal system is directly traceable to the non-symmorphic space group symmetry of Netsene ($I4/mcm$) and the specific half-lattice-constant shift between layers dictated by our design principle. The screw axis $\{C_{2z}|(\frac{1}{2},\frac{1}{2},0)\}$ and glide mirror $\{M_y|(\frac{1}{2},\frac{1}{2},0)\}$ protect the band crossings along high-symmetry lines and enforce the formation of extended nodal surfaces rather than isolated lines or points. The π-orbital hybridization pattern, modulated by the shifted stacking and the sp^3 connectors, generates precisely the number of closely spaced bands necessary for this complex degeneracy. A non-trivial $\mathbb{Z}_2$ topological invariant, evaluated from the Berry phase on a loop encircling any of these nodal surfaces, guarantees their topological protection [5].

A direct spectroscopic signature of this nested nodal-surface system appears in the electronic DOS. As seen in Fig. 4(b), a pronounced peak emerges just above E_F. This peak corresponds to a van Hove singularity arising from the extended regions of nearly flat dispersion associated with the nodal surfaces. This feature is highly reminiscent of the physics of TBG, where flat bands and van Hove singularities arise from Moiré superlattice potentials. In a conceptual sense, Netsene can be compared with magic-angle TBG: whereas TBG uses a rotational misorientation to generate real-space Moiré flat bands, Netsene employs a translational layer shift permanently fixed by covalent bonds to generate momentum-space nodal surfaces with an attendant high DOS. This analogy suggests that Netsene is a promising structural platform for investigating possible correlation effects in a bulk setting, warranting future theoretical studies. Moreover, the

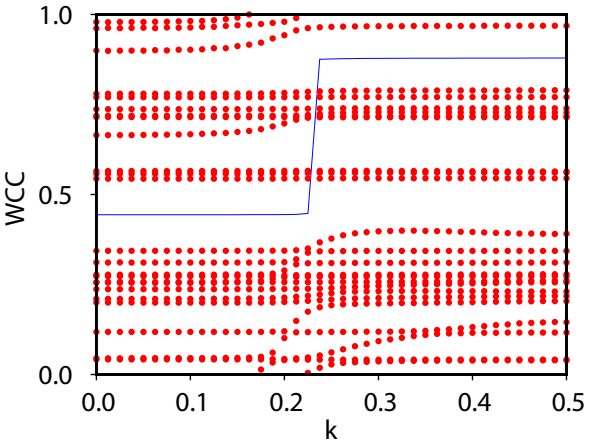


FIG. 6: WCC evolution on the six time-reversal invariant momentum planes of Netsene. The five planes $k_1 = 0.0$, $k_1 = 0.5$, $k_2 = 0.0$, $k_2 = 0.5$, and $k_3 = 0.0$ exhibit trivial WCCs flow ($\mathbb{Z}_2 = 0$), while the $k_3 = 0.5$ plane shows non-trivial winding with an odd number of crossings of an arbitrary reference line ($\mathbb{Z}_2 = 1$), yielding a three-dimensional $\mathbb{Z}_2$ index of $(0; 001)$.

multi-band nodal-surface topology and the high density of states near E_F may lead to anisotropic transport and unusual Hall responses, which are attractive directions for future experimental and theoretical exploration.

D. Topological invariant and symmetry protection of the nodal surface

To rigorously establish the topological nature of the observed nodal degeneracies, we have performed Wilson-loop calculations, Berry-phase evaluations [20, 28], and an irreducible representation (irrep) [29] analysis of the bands involved.

As shown in Fig. 6, the WCCs evolution on the five planes $k_1 = 0.0$, $k_1 = 0.5$, $k_2 = 0.0$, $k_2 = 0.5$, and $k_3 = 0.0$ is topologically trivial ($\mathbb{Z}_2 = 0$), exhibiting no crossing of an arbitrary reference line. In contrast, on the $k_3 = 0.5$ plane, the WCCs flow displays non-trivial behavior ($\mathbb{Z}_2 = 1$), with the WCC lines crossing the reference line an odd number of times. The resulting three-dimensional $\mathbb{Z}_2$ topological index is therefore $(0; 001)$. By the bulk-boundary correspondence, the non-trivial $\mathbb{Z}_2$ index $(0; 001)$ implies the existence of topological drumhead surface states on the (001) surface, consistent with the nodal-surface character.

This result is fully consistent with the nodal-surface semimetal picture. In topological semimetals, band degeneracies can be classified by their dimensionality: zero-dimensional nodal points, one-dimensional nodal lines, and two-dimensional nodal surfaces. Unlike point or line degeneracies, a nodal surface extends continuously over a two-dimensional manifold in momentum space. In a three-dimensional Brillouin zone, such a two-dimensional nodal surface corresponds, along its normal direction, to a specific k plane, precisely the $k_3 = 0.5$ plane on which we observe the non-trivial $\mathbb{Z}_2 = 1$ invariant. This non-trivial topological index reflects the non-trivial winding of the bulk wave functions on that plane and constitutes a direct manifestation of the nodal-surface topology.

To further elucidate the symmetry origin of the degeneracies, we performed an irreducible representation (irrep) analysis of the bands forming the nodal surface. At a representative k-point on the crossing, the band above the E_F transforms as B_1 and band below the E_F as B_2. According to group theory, bands with different irreps are allowed to cross without hybridizing; the degeneracy is therefore an accidental band crossing protected by C_2 symmetry. Such symmetry-protected accidental crossings are the fundamental building blocks of nodal-line and nodal-surface semimetals, and they remain robust against any perturbation that preserves the C_2 symmetry.

Taken together, the WCCs evolution, the non-trivial $\mathbb{Z}_2$ index $(0; 001)$, and the C_2-protected accidental band crossing (B_1/B_2 irreps) provide convergent evidence that Netsene possesses a non-trivial topological electronic structure and belongs to the class of nodal-surface semimetals. This discovery establishes Netsene as an ideal platform for investigating higher-dimensional topological degeneracies and their associated physical properties.

IV. SUMMARY

In summary, we have proposed and validated a general symmetry-engineering principle that systematically transforms the Dirac cone of 2D graphene into a 3D nested nodal-surface semimetal. Guided by this principle and accelerated by a deep generative model, we have revealed that Netsene — hosts a complex nested nodal-surface system around the E_F, accompanied by Dirac-like linear crossings with Fermi velocities comparable to graphene. Its non-trivial bulk topology is confirmed by topological invariants and symmetry analysis, and is expected to manifest in drumhead surface states. The combination of high Fermi velocity (comparable to graphene), topological nodal surfaces, high mechanical stiffness ($C_{33} = 1134.2$ GPa), and robust stability positions Netsene as a compelling 3D carbon platform. As a structure that shares certain flat-band characteristics with TBG, Netsene offers a rigid bulk system for studying correlation physics in future works and may hold potential for high-speed electronic applications.Furthermore, the distinctive Fermi-surface topology associated with the nested nodal surfaces may give rise to unique transport signatures, including direction dependent magnetoresistance and possible anomalous Hall contributions; a quantitative investigation of these transport properties is an interesting direction for future study. This work demonstrates the power of theory-guided, machine-

learning-accelerated materials identification for engineering exotic topological quantum phases, and highlights the value of revisiting known materials with new theoretical frameworks.

Acknowledgments. We wish to thank K. Bu and D.-X. Yao for helpful discussions. We are grateful to Davide M. Proserpio for bringing the SACADA database and the prior report of Netsene to our attention. This work is supported by Natural Science Foundation of Hebei Province (Grant No. A2026203033), Beijing National Laboratory for Condensed Matter Physics (Grant No. 2024BNLCMPKF020), Innovation Capability Improvement Project of Hebei province (Grant No. 22567605H) and the National Natural Science Foundation of China (Grants No.12204400).

[1] Novoselov K S, Geim A K, Morozov S V, Jiang D, Zhang Y, Dubonos S V, Grigorieva I V and Firsov A A 2004 *Science* **306** 666–669 ISSN 1095-9203
[2] Castro Neto A H, Guinea F, Peres N M R, Novoselov K S and Geim A K 2009 *Reviews of Modern Physics* **81** 109–162
[3] Burkov A A and Balents L 2011 *Physical Review Letters* **107** 127205
[4] Armitage N P, Mele E J and Vishwanath A 2018 *Reviews of Modern Physics* **90** 015001
[5] Wu W, Liu Y, Li S, Zhong C, Yu Z M, Sheng X L, Zhao Y X and Yang S A 2018 *Physical Review B* **97** 115125
[6] Bzdušek T and Sigrist M 2017 *Physical Review B* **96** 155105
[7] Wang J T, Nie S, Weng H, Kawazoe Y and Chen C 2018 *Physical Review Letters* **120** 026402
[8] Wang J T, Weng H and Chen C 2019 *Advances in Physics: X* **4** 1625724 ISSN null
[9] Xie T, Fu X, Ganea O E, Barzilay R and Jaakkola T 2021 *International Conference on Learning Representations (ICLR)* (*Preprint* 2110.06197)
[10] Cao Z, Luo X, Lv J and Wang L 2025 *Science Bulletin* **70** 3522–3533 ISSN 2095-9273
[11] Dong X, Hu M, He J, Tian Y and Wang H T 2015 *Scientific Reports* **5** 10713
[12] Cao Y, Fatemi V, Fang S, Watanabe K, Taniguchi T, Kaxiras E and Jarillo-Herrero P 2018 *Nature* **556** 43–50
[13] Bistritzer R and MacDonald A H 2011 *Proceedings of the National Academy of Sciences* **108** 12233–12237 ISSN 0027-8424, 1091-6490
[14] Liu Z, Li Y and Yang Y F 2019 *Chinese Physics B* **28** 077103 ISSN 1674-1056
[15] Cheng C, Zhang X, Ma S and Wang S 2023 *Physical Chemistry Chemical Physics* **25** 13116–13125 ISSN 1463-9084
[16] Bu K, Wang J T, Weng H and Chen C 2020 *Physical Review B* **101** 205104
[17] Bu K, Qian Y, Wang J T and Weng H 2021 *Physical Review B* **103** L081108
[18] Wang J T, Bu K, Qian Y, Weng H and Chen C 2021 *Physical Review B* **104** 245143
[19] Jiang W, Jiang J, Zhang Z, Wu W, Zhang L C, Xie Y and Chen Y 2024 *Nanoscale* **16** 13543–13550 ISSN 2040-3372
[20] Wu Q, Zhang S, Song H F, Troyer M and Soluyanov A A 2018 *Computer Physics Communications* **224** 405–416 ISSN 0010-4655
[21] Sofo J O, Chaudhari A S and Barber G D 2007 *Physical Review B* **75** 153401
[22] Yuan X, Liu J, Liu J, Wei J, Chen L, Wang W and Li C 2024 *Diamond and Related Materials* **149** 111625 ISSN 0925-9635
[23] Jain A, Ong S P, Hautier G, Chen W, Richards W D, Dacek S, Cholia S, Gunter D, Skinner D, Ceder G and Persson K A 2013 *APL Materials* **1** 011002 ISSN 2166-532X
[24] Hoffmann R, Kabanov A A, Golov A A and Proserpio D M 2016 *Angewandte Chemie International Edition* **55** 10962–10976
[25] Giannozzi P, Andreussi O, Brumme T, Bunau O, Nardelli M B, Calandra M, Car R, Cavazzoni C, Ceresoli D, Cococcioni M, Colonna N, Carnimeo I, Corso A D, Gironcoli S d, Delugas P, DiStasio R A, Ferretti A, Floris A, Fratesi G, Fugallo G, Gebauer R, Gerstmann U, Giustino F, Gorni T, Jia J, Kawamura M, Ko H Y, Kokalj A, Küçükbenli E, Lazzeri M, Marsili M, Marzari N, Mauri F, Nguyen N L, Nguyen H V, Otero-de-la Roza A, Paulatto L, Poncé S, Rocca D, Sabatini R, Santra B, Schlipf M, Seitsonen A P, Smogunov A, Timrov I, Thonhauser T, Umari P, Vast N, Wu X and Baroni S 2017 *Journal of Physics: Condensed Matter* **29** 465901 ISSN 0953-8984
[26] Perdew J P, Burke K and Ernzerhof M 1996 *Physical Review Letters* **77** 3865–3868 ISSN 1079-7114
[27] Mostofi A A, Yates J R, Lee Y S, Souza I, Vanderbilt D and Marzari N 2008 *Computer Physics Communications* **178** 685–699 ISSN 0010-4655
[28] Xiao D, Chang M C and Niu Q 2010 *Reviews of Modern Physics* **82** 1959–2007
[29] Bradlyn B, Elcoro L, Cano J, Vergniory M G, Wang Z, Felser C, Aroyo M I and Bernevig B A 2017 *Nature* **547** 298–305 ISSN 1476-4687
[30] Yu R, Qi X L, Bernevig A, Fang Z and Dai X 2011 *Physical Review B* **84** 075119
[31] Li Z Z, Lian C S, Xu J, Xu L F, Wang J T and Chen C F 2015 *Phys. Rev. B* **91** 214106
[32] Wang J T, Weng H, Nie S, Fang Z, Kawazoe Y and Chen C F 2016 *Phys. Rev. Lett.* **116** 195501
[33] Li Z Z, Chen J, Nie S, Xu L, Mizuseki H, Weng H and Wang J T 2018 *Carbon* **133** 39–43 ISSN 0008-6223
[34] David W I F, Ibberson R M, Matthewman J C, Prassides K, Dennis T J S, Hare J P, Kroto H W, Taylor R and Walton D R M 1991 *Nature* **353** 147–149
[35] Malko D, Neiss C, Vines F and Gorling A 2012 *Physical Review Letters* **108** 086804
[36] Fan Q, Yan L, Tripp M W, Krejcí O, Dimosthenous S, Kachel S R, Chen M, Foster A S, Koert U, Liljeroth P and Gottfried J M 2021 *Science* **372** 852–856 ISSN 0036-8075, 1095-9203
[37] Maultzsch J, Reich S, Thomsen C, Requardt H and Ordejon P 2004 *Phys. Rev. Lett.* **92** 075501
[38] McSkimin H J and Andreatch P 1972 *Journal of Applied Physics* **43** 2944–2948

[39] Bosak A, Krisch M, Mohr M, Maultzsch J and Thomsen C 2007 *Physical Review B* **75** 153408

[40] Deacon R S, Chuang K C, Nicholas R J, Novoselov K S and Geim A K 2007 *Physical Review B* **76** 081406